










Comparative structural evolution under pressure of powder and single crystals of the layered antiferromagnet FePS₃

David M. Jarvis ^{1,2} Matthew J. Coak ^{3,2} Hayrullo Hamidov ^{2,4} Charles R. S. Haines ^{5,2} Giulio I. Lampronti,⁶
Cheng Liu ² Shiyu Deng ² Dominik Daisenberger,⁷ David R. Allan ⁷ Mark R. Warren,⁷
Andrew R. Wildes ^{1,*} and Siddharth S. Saxena ^{2,†}

¹*Institut Laue-Langevin, 71 Avenue des Martyrs, 38042 Grenoble, France*

²*Cavendish Laboratory, University of Cambridge, J. J. Thomson Avenue, Cambridge CB3 0HE, United Kingdom*


³*Department of Physics, University of Warwick, Gibbet Hill Road, Coventry CV4 7AL, United Kingdom*

⁴*Navoi State University of Mining and Technologies, 72 M. Tarobiy Street, Navoi 210100, Uzbekistan*

⁵*Physics, University of East Anglia, Norwich NR4 7TJ, United Kingdom*

⁶*Department of Earth Sciences, University of Cambridge, Downing Street, Cambridge CB2 3EQ, United Kingdom*

⁷*Diamond Light Source, Chilton, Didcot OX11 0DE, United Kingdom*

 (Received 24 February 2022; revised 7 July 2022; accepted 12 January 2023; published 14 February 2023)

FePS₃ is a layered magnetic van der Waals compound that undergoes a Mott insulator-metal transition under applied pressure. The transition has an associated change in the crystal symmetry and magnetic structure. Understanding the underlying physics of these transitions requires a detailed understanding of the crystal structure as a function of pressure. Two conflicting models have previously been proposed for the evolution of the structure with pressure. To settle the disagreement, we present a study of the pressure-dependent crystal structures using both single-crystal and powder x-ray diffraction measurements. We show unambiguously that the highest-pressure transition involves a collapse of the interplanar spacing, along with an increase in symmetry from a monoclinic to a trigonal space group, to the exclusion of other models. Our collected results are crucial for understanding high-pressure behavior in these materials and demonstrate a clear and complete methodology for exploring complex two-dimensional material structures under pressure.

DOI: [10.1103/PhysRevB.107.054106](https://doi.org/10.1103/PhysRevB.107.054106)

I. INTRODUCTION

Two-dimensional materials whose layers are only weakly connected by van der Waals (vdW) bonding have emerged as systems of considerable current interest both from the point of view of their fundamental properties and the possibility to exploit them in nanoscale multifunctional devices, transistors, spintronic gates, and sensors. In recent years a number of material families have gained renewed interest as their magnetic and electronic interactions are intertwined, putting them firmly in the realm of quantum materials research. These systems are quasi-two-dimensional in bulk but can be delaminated, allowing for the exciting possibility of understanding correlated quantum systems all the way from a bulk sample down to a single atomic layer.

The MPS₃ materials (M = first row 2+ transition metal) form one such family. Under ambient pressure they are antiferromagnetic Mott insulators with a common monoclinic structure, space group $C2/m$, consisting of near-perfect honeycomb layers of transition metal ions in the ab planes [1,2]. The weak coupling between the planes extends to both the structural and magnetic properties, making them a good approximation of a two-dimensional magnetic system. They can

be delaminated down to a monolayer, making them ideal model materials in which to explore two-dimensional magnetic systems and associated correlated electron physics [3].

Complementary to thickness-control studies, a reduction of the interlayer spacing may give rise to a more three-dimensional structure, changing the magnetic and transport properties. The application of hydrostatic pressure is an excellent, targeted technique for tuning in this manner. When applied to stoichiometric compounds, it provides a cleaner avenue to study exotic phenomena in other low-dimensional materials [4], for example, the pseudogap phase in high-temperature superconductors. Indeed, studies on MPS₃ have demonstrated the presence of Mott insulator-to-metal transitions [5] and even the emergence of superconductivity in FePSe₃ [6].

The insulator-to-metal transition in FePS₃ occurs at a pressure of 14 GPa. The transition is accompanied by changes in the magnetic properties [6,7] and by changes in the crystal structure. Precise knowledge of the pressure-dependent crystal structure is essential for a fundamental understanding of the novel electronic and magnetic properties. X-ray diffraction with synchrotron radiation is an appropriate method for such a study. The evolution of the crystal structure of powdered FePS₃ as a function of pressure has previously been studied using x-ray diffraction by two groups [6,8], however, the interpretations of the data are contradictory. The studies agree that the insulator-metal transition is accompanied by a volume

*Corresponding author: wildes@ill.fr

†Corresponding author: sss21@cam.ac.uk

collapse in the unit cell, but the proposed models for the structures are very different.

Haines *et al.* [8] propose that FePS₃ undergoes two structural phase transitions up to 30 GPa. The first, at a critical pressure of 4 GPa, is characterized as a shear of the weakly coupled *ab* planes along the crystallographic *a* direction, maintaining the ambient-pressure *C2/m* space group while reducing the angle β to very nearly 90°. The second transition occurs at 14 GPa, concomitant with the insulator-metal transition. The volume collapse is due to a dramatic reduction of the interplanar spacing with a simultaneous symmetry increase to a trigonal *P* $\bar{3}1m$ space group.

Wang *et al.* [6] propose that there is no change of the crystallographic space group and the *C2/m* is maintained at all pressures, with no large change in β . They attribute the volume collapse to a discontinuous reduction in the *a* and *b* lattice parameters, requiring a shrinking of the Fe²⁺ honeycombs. They furthermore present indirect results on the magnetism from x-ray emission spectroscopy suggesting that the compound becomes nonmagnetic, which contradicts neutron diffraction measurements that show a nonzero sublattice moment with short-ranged order [7].

Further experiments are required to determine unambiguously the pressure-dependent crystal structure of FePS₃ both to resolve the contradictions between the two groups and for *ab initio* calculations of the physical properties [9,10]. We report here a comprehensive study examining the evolution of the crystal structure under pressure of FePS₃ by diffraction of synchrotron radiation, and are able uniquely to draw robust conclusions without relying on any choice of model to interpret or fit the raw data. We show new data from both single-crystal and powder samples in diamond anvil cells with a helium pressure transmitting medium, and compare these new data with previously published measurements [8] of powder samples without a pressure medium. The highest-pressure transition is found in all cases to include an increase in symmetry to a trigonal *P* $\bar{3}1m$ structure and a collapse of the interplanar spacing. The extent of this *c*-axis collapse is found to be sensitive to the presence of a helium pressure-transmitting medium, being greatest in experiments without such a medium, showing that careful consideration of the sample environment is necessary for the understanding of the high-pressure behavior of this material. Our conclusions will allow accurate *ab initio* calculations of the electronic and magnetic properties, and the methodology we employ provides a general template for structural studies of similar compounds at high pressures.

II. METHODS

Single crystals of FePS₃ were grown by a vapor transport method as described in detail in Ref. [11]. Samples were manually delaminated down to a thickness of ~ 15 μm and cut to squares of side length 80 μm . Single-crystal x-ray diffraction data were collected at room temperature on the I19-2 beamline at the Diamond Light Source. An incident beam of wavelength 0.4859 Å ($E = 25$ keV) was used to collect diffraction patterns using a Dectris Pilatus 300K detector. The platelet samples were mounted such that the *c** axis was approximately parallel to the incident beam. Data were then

collected as the crystal was rotated about ϕ and ω in a standard configuration. The data were analyzed using CRYSTALIS PRO software [12].

Powder samples were prepared by grinding the as-grown crystals under liquid nitrogen in order to mitigate the noted tendency towards strong preferred orientations in these materials. This preparation is identical to that used in previous work [8]. Powder x-ray diffraction measurements at room temperature were performed on the I15 Extreme Conditions beamline at the Diamond Light Source. X rays of wavelength 0.4246 Å ($E = 29.2$ keV) were used with a MAR345 area detector. The data were initially processed using DAWN software [13] with Rietveld and Le Bail refinements performed using TOPAS [14] and GSAS-II [15]. Full details and discussion of the data treatment and refinement, as well as raw data and analysis and comparisons of the models employed in the literature are shown in the Supplemental Material [16] and references therein [17–23].

Rhenium gaskets were used with the diamond anvil cells of culet size 400 μm for both experiments, and the cells were loaded with helium gas as a pressure-transmitting medium. Load was applied using a gas loading membrane system. The pressure inside the sample space was determined by measurement of the fluorescence of ruby spheres inserted alongside the sample [24]. We estimated the uncertainties on pressure values to be approximately ± 0.2 GPa, based on the width of the fluorescence peak and on measuring separate ruby spheres at differing locations within the sample environment.

Diffraction peaks arising from the diamond anvils were identified by fitting the known diamond unit cell and were removed from subsequent treatment. Regions of detector images containing powderlike rings from the rhenium gasket were also identified, and were excluded from refinements.

III. RESULTS

Both the powder and single-crystal data confirm the presence of the two structural phase transitions observed by Haines *et al.* [8]. The three phases are hereafter designated HP-0, HP-I, and HP-II for the ambient-, intermediate-, and high-pressure regimes, respectively. The transition from HP-0 to HP-I occurred at 4 GPa while the transition from HP-I to HP-II occurred at 14 GPa. Analysis confirmed the conclusions of Haines *et al.* [8], that the HP-I phase has a space group *C2/m* with $\beta \approx 90^\circ$ and the HP-II phase had a higher-symmetry trigonal *P* $\bar{3}1m$ space group. All the transitions were abrupt with no clear evidence of phase coexistence. Unit-cell and single-crystal refinement parameters for each phase are given in Table I. Complementary parameters from refining the powder data are shown in Tables S1–S3 in the Supplemental Material [16].

The data show unambiguously that the volume collapse at the HP-I to HP-II transition is due to a dramatic reduction in the interlayer spacing between the *ab* planes. This conclusion is clear from an observation of the positions of the 00*l* peaks which give a direct measure of the interlayer distance. These peaks, in particular 001, are visible in the powder data. The analysis relies on the correct indexing of diffraction peaks. Refinements using the model of Wang *et al.*, with the same *C2/m* space group, were possible but led to a misidentification

TABLE I. Lattice parameters, space groups, completeness, and R_{int} for the three identified phases as determined from single crystal data using CRYSTALIS PRO.

		a (Å)	b (Å)	c (Å)	β (deg)	Comp.	R_{int}
Ambient/HP-0 (1.2 GPa)	$C2/m$	5.80(1)	10.030(6)	7.1(1)	106.9(7)	37.99%	0.1256
HP-I (6.7 GPa)	$C2/m$	5.802(2)	10.056(4)	5.95(7)	90.0(1)	26.97%	0.0880
HP-II (20.1 GPa)	$P31m$	5.665(4)		5.02(9)		30.83%	0.2056

of the 001 peak in the HP-II phase, and an overall structure which was clearly incompatible with the single-crystal data.

Definitive proof of the collapse of the interlayer spacing comes from the single-crystal measurements. The 001 peak was not accessible in the single-crystal measurements due to the experimental geometry. However, peaks at $0kl$ were accessible and provide clear measures of lattice spacings. The \mathbf{b}^* and \mathbf{c}^* directions are orthogonal in all the considered space groups, being in and normal to the ab planes, respectively. The separation in l , expressed in \AA^{-1} , gives the interlayer spacing, and the positions in k , again in \AA^{-1} , give a characteristic intraplanar distance. These values are independent of the choice of space group, thus giving model-free lattice spacings.

Figure 1 shows slices of the $(0kl)$ scattering planes generated from single-crystal diffraction data at three pressures corresponding to the HP-0, HP-I, and HP-II regimes. Strong monoclinic $06l$ and $0\bar{6}l$ peaks for $l = -1, 0, 1$, which are instead indexed in HP-II as $0 - 3l$ and $03l$ respectively visible alongside powder rings from the rhenium gasket. Smearing of the strongest Bragg peaks parallel to the \mathbf{c}^* direction is attributable to stacking faults and the quasi-two-dimensional nature in this family of materials [17,25,26]. These slices show a distinct increase in the separation of the peaks along the \mathbf{c}^* direction between the HP-I and HP-II phases, corresponding to a reduction in the interplanar distance, without a similar change in the $0k0$ distances. This is unambiguous evidence that the volume reduction upon the transition to HP-II is due to changes in the separation between the planes, rather than an intraplanar change of the honeycombs themselves.

The characteristic inter- and intralayer spacings extracted from the Le Bail (powder) and single-crystal (CRYSTALIS PRO) refinements, based on the Haines *et al.* model, and from the model-free fitting of the peak positions in the $(0kl)$ slices are shown in Figs. 2 and 3, respectively. The data analysis methods are described in the Supplemental Material. The transition from the HP-0 to the HP-I phase is not clearly observable in the figures as this transition involves a shear along the \mathbf{a} axis, with a minimal change in the characteristic spacings, but is apparent in a change in intensities for the powder data around

the 131 and $20\bar{2}$ peaks as shown in Fig. S4 in the Supplemental Material [16].

The HP-I to HP-II transition is clearly observed in all data sets at 14 GPa and, as shown in Fig. 2, in all cases involves a reduction of the interplanar distance. The evolution of the interplanar spacing, including the magnitude of the reduction at 14 GPa, agree quantitatively at all pressures between the single-crystal and powder data analysis. A line showing a fit of the data in the HP-II phase is shown in the figure.

The previously published data of Haines *et al.* have also been included in this figure, showing the same discontinuous change at the same critical pressure. There is a quantitative difference in the magnitude of the change which may be attributed to the use of a pressure medium. A helium medium was used for the current data where none was used by Haines *et al.* The data of Haines *et al.* in the HP-II phase are visibly lower and flatter than the current data, as is apparent from a comparison with the linear fit to the current data. The no-medium data show a greater reduction at the phase transition, with a change of 13.5% from 5.72(1) to 4.95(1) \AA , while the data sets taken with a helium medium show a mean reduction of 11.7%, from 5.79(3) to 5.2(1) \AA .

The characteristic intraplanar distances are shown in Fig. 3. The distances may be correlated to the nearest-neighbor distances between Fe^{2+} ions in the honeycombs shown in the inset of the figure. In the limit of a perfect honeycomb structure, which is almost exact for FePS_3 at ambient pressure [1], the spacing of these $(0k0)$ planes is equal to half the side length of a hexagon. The single-crystal data match quantitatively with the results from Haines *et al.* The data show that the characteristic intraplanar spacing does not display a significant discontinuity across any of the transitions. However, a discontinuity is observed in the gradient of this value with pressure across the HP-II transition, with the in-plane distance being more resistant to compression in the HP-II phase. The absence of a discontinuous change, combined with the observation of the collapse shown in Fig. 2, shows unambiguously that the volume collapse is due to the interlayer spacing.

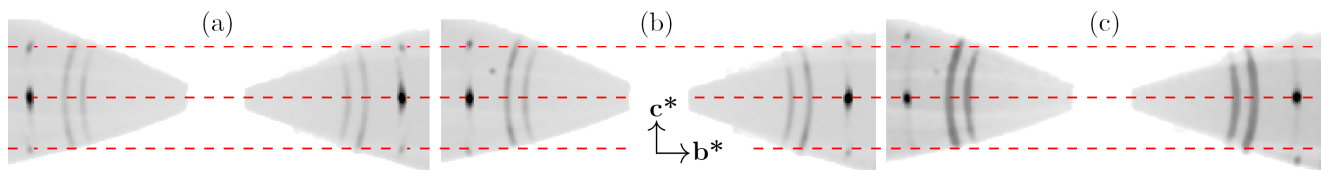


FIG. 1. Reciprocal space image of the $(0kl)$ scattering plane in single-crystal FePS_3 in the three distinct structural phases at (a) 1.2 GPa, (b) 6.7 GPa, and (c) 19.1 GPa. Visible spots in the lower two pressures are indexed with $k = \pm 6$ and in the highest pressure as $k = \pm 3$. The dashed lines from bottom to top indicate the lowest-pressure position of the $0k\bar{1}$, $0k0$, and $0k1$ lines, illustrating the increase in $Q_{(001)}$ with pressure.

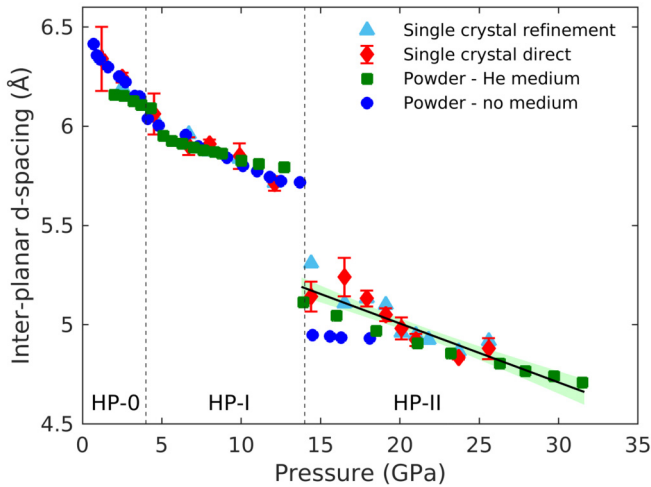


FIG. 2. d spacing of the 001 diffraction peak, corresponding to the interlayer separation in FePS_3 in (cyan) single-crystal refinement; (red) single crystal as determined from $(0kl)$ images; (green) powder sample with a He pressure medium; (blue) powder x-ray diffraction data without a pressure medium of Haines *et al.* [8]. The black line shows a linear fit to the HP-II values of all measurements using a He pressure medium and the shaded region the associated 95% confidence intervals as determined by the MATLAB fit.

The determination of the intraplanar distances from the new powder data with the helium medium was ambiguous due to an experimental constraint limiting the detector angle range that provided usable data. Although the intraplanar distance could be reliably determined as the 001 peak appears at a small scattering angle, reliable values for the in-plane lattice dimensions could not be extracted in the HP-0 and HP-I

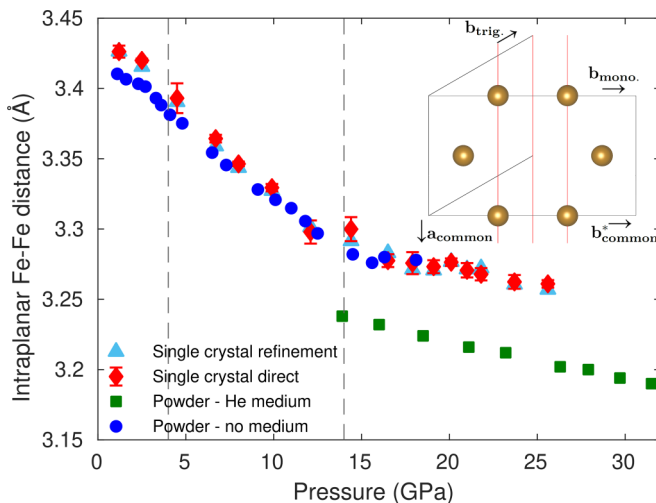


FIG. 3. Average intraplanar nearest-neighbor distance between Fe ions as a function of pressure as determined from (cyan) single-crystal refinement; (red) single crystal as determined from $(0kl)$ and equivalent images; (green) powder sample with a He pressure medium; (blue) powder diffraction without pressure medium. Inset: Fe cations in the ab planes of the monoclinic and trigonal unit cells as viewed along the c^* axis. The spacing of the (060) monoclinic or (030) trigonal lattice planes is shown in red.

phases due to covariance between the refinement parameters. Full details are provided in Sec. 6 of the Supplemental Material. Hence, only values for the trigonal HP-II phase, where $a = b$, are shown in Fig. 3. The gradient for the new powder data matches those of the other experiments but there is a difference in the magnitudes. Given the similar behavior for all the data observed in Fig. 2, there is no reason to doubt that the gradient in the HP-0 and HP-I phases also matches the other experiments and that no discontinuity is present at the HP-II transition.

IV. DISCUSSION

Our results verify the structural model determined by Haines *et al.* and prove that the volume collapse at the HP-I to HP-II transition is due to a discontinuous change in the interplanar spacing. Our conclusions are unambiguous and apparent due to the use of a model-free method measuring the reciprocal-space distances between Bragg peaks that are clearly correlated with specific, characteristic spacings in the unit cell. Our results provide a foundation for future *ab initio* calculations on FePS_3 , and the methodology employed establishes a template for rigorous high-pressure structural studies on related low-dimensional compounds such as M -dichalcogenides [27], MI_3 [28], $MP(S, \text{Se})_3$ [5,6], MnSb_2Te_4 [29], CrGeTe_3 [30], and CrPS_4 [31].

The magnitudes of the high-pressure lattice parameters show differences between the data sets taken under different conditions. This is particularly evident for the powder data with a helium pressure medium in Fig. 3, and is also true for data ≤ 20 GPa in the HP-II phase in Fig. 2. There are two potential factors influencing this behavior which are immediately suggested: the presence of a helium pressure medium and the form of the sample.

The pressure-transmitting medium allows a more hydrostatic pressure distribution in the sample. It is noteworthy that no phase coexistence was observed in the new data with a helium pressure medium, but a significant phase coexistence was observed in the data of Haines *et al.* where no pressure medium was used. Inhomogeneity in the local pressure in the absence of a transmitting medium may explain this disparity. The effect of a more significant uniaxial component of pressure on the interplanar spacing and volume collapse warrants further investigation.

A more subtle effect may be the interaction of helium itself with FePS_3 . The intercalation of MPS_3 materials with elements such as lithium [32] has been found to strongly affect both the electronic and magnetic properties. The differences seen in Fig. 3 between the single-crystal and powder data, both with a helium medium, could then arise from differing amounts of intercalation into the material with the intercalation being more complete in the powder sample. Similar effects have been seen when intercalating graphite with Li [33] or Yb [34] where the intercalation was limited to the edges of the sample.

Potential effects due to structural transitions in the helium pressure medium are likely minor for our overall conclusions. Helium solidifies at 300 K and 11.5 GPa [35], which is sufficiently far from the HP-I to HP-II transition that any influence can be disregarded, and solid helium remains extremely soft in

comparison to the sample itself. X-ray studies of the structural evolution under pressure of the related compound $V_{0.9}PS_3$ showed no effect of the helium solidification [36].

Regardless of the microscopic origins, the quantitative differences between measurements made under different conditions cannot be ignored. They are direct evidence that the high-pressure properties of these types of material are sensitive to experimental factors. Theoretical calculations must make careful consideration of the sample conditions when using experimental data as a basis for the determination of properties such as band structures.

V. CONCLUSION

In conclusion, we determine and confirm a detailed model of the structural transition linked to metallization and new magnetic states in HP-II $FePS_3$. This transition involves a symmetry increase from space group $C2/m$ to $P\bar{3}1m$ and a significant volume collapse due to a reduction of interplanar spacing. By drawing together data under multiple experimen-

tal conditions and using symmetry arguments to analyze raw data, we are able to categorically rule out other models proposed. We find that the extent of the collapse is sensitive to the use of a helium pressure medium and note that consideration must be given to these factors in future experiments and calculations.

ACKNOWLEDGMENTS

This research was supported by United Kingdom Research and Innovation Global Challenges Research Fund COMPASS Grant No. ES/P010849/1 and Cambridge Central Asia Forum, Jesus College, Cambridge. This project has received funding from the U.K. Department of Business, Environment and Industrial Strategy (BEIS) to support collaboration between the Cavendish Laboratory and Navoi State University of Mining and Technologies. We thank the British Embassy in Tashkent for their support. This work was carried out with the support of the Diamond Light Source through the award of beamtime for Proposals No. EE15949 and No. CY23524.

-
- [1] G. Ouvrard, R. Brec, and J. Rouxel, Structural determination of some MPS_3 layered phases ($M = Mn, Fe, Co, Ni$ and Cd), *Mater. Res. Bull.* **20**, 1181 (1985).
- [2] R. Brec, Review on structural and chemical properties of transition metal phosphorous trisulfides MPS_3 , *Solid State Ionics* **22**, 3 (1986).
- [3] J.-G. Park, Opportunities and challenges of 2D magnetic van der Waals materials: Magnetic graphene? *J. Phys.: Condens. Matter* **28**, 301001 (2016).
- [4] A. F. Kusmartseva, B. Sipos, H. Berger, L. Forró, and E. Tutiš, Pressure Induced Superconductivity in Pristine $1T$ - $TiSe_2$, *Phys. Rev. Lett.* **103**, 236401 (2009).
- [5] M. J. Coak, D. M. Jarvis, H. Hamidov, C. R. S. Haines, P. L. Alireza, C. Liu, S. Son, I. Hwang, G. I. Lampronti, D. Daisenberger, P. Nahai-Williamson, A. R. Wildes, S. S. Saxena, and J.-G. Park, Tuning dimensionality in van-der-Waals antiferromagnetic Mott insulators $TMPS_3$, *J. Phys.: Condens. Matter* **32**, 124003 (2020).
- [6] Y. Wang, J. Ying, Z. Zhou, J. Sun, T. Wen, Y. Zhou, N. Li, Q. Zhang, F. Han, Y. Xiao, P. Chow, W. Yang, V. V. Struzhkin, Y. Zhao, and H.-k. Mao, Emergent superconductivity in an iron-based honeycomb lattice initiated by pressure-driven spin-crossover, *Nat. Commun.* **9**, 1914 (2018).
- [7] M. J. Coak, D. M. Jarvis, H. Hamidov, A. R. Wildes, J. A. M. Paddison, C. Liu, C. R. S. Haines, N. T. Dang, S. E. Kichanov, B. N. Savenko, S. Lee, M. Kratochvílová, S. Klotz, T. C. Hansen, D. P. Kozlenko, J.-G. Park, and S. S. Saxena, Emergent Magnetic Phases in Pressure-Tuned van der Waals Antiferromagnet $FePS_3$, *Phys. Rev. X* **11**, 011024 (2021).
- [8] C. R. S. Haines, M. J. Coak, A. R. Wildes, G. I. Lampronti, C. Liu, P. Nahai-Williamson, H. Hamidov, D. Daisenberger, and S. S. Saxena, Pressure-Induced Electronic and Structural Phase Evolution in the van der Waals Compound $FePS_3$, *Phys. Rev. Lett.* **121**, 266801 (2018).
- [9] Y. Zheng, X.-x. Jiang, X.-x. Xue, J. Dai, and Y. Feng, *Ab initio* study of pressure-driven phase transition in $FePS_3$ and $FePSe_3$, *Phys. Rev. B* **100**, 174102 (2019).
- [10] R. A. Evarestov and A. Kuzmin, Origin of pressure-induced insulator-to-metal transition in the van der Waals compound $FePS_3$ from first-principles calculations, *J. Comput. Chem.* **41**, 1337 (2020).
- [11] D. Lançon, H. C. Walker, E. Ressouche, B. Ouladdiaf, K. C. Rule, G. J. McIntyre, T. J. Hicks, H. M. Rønnow, and A. R. Wildes, Magnetic structure and magnon dynamics of the quasi-two-dimensional antiferromagnet $FePS_3$, *Phys. Rev. B* **94**, 214407 (2016).
- [12] CRYSTALIS PRO, Agilent Technologies, Ltd. (2014).
- [13] J. Filik, A. W. Ashton, P. C. Y. Chang, P. A. Chater, S. J. Day, M. Drakopoulos, M. W. Gerring, M. L. Hart, O. V. Magdysyuk, S. Michalik, A. Smith, C. C. Tang, N. J. Terrill, M. T. Wharmby, and H. Wilhelm, Processing two-dimensional X-ray diffraction and small-angle scattering data in DAWN 2, *J. Appl. Crystallogr.* **50**, 959 (2017).
- [14] A. A. Coelho, TOPAS and TOPAS-ACADEMIC: An optimization program integrating computer algebra and crystallographic objects written in C++, *J. Appl. Crystallogr.* **51**, 210 (2018).
- [15] B. H. Toby and R. B. Von Dreele, GSAS-II: The genesis of a modern open-source all purpose crystallography software package, *J. Appl. Crystallogr.* **46**, 544 (2013).
- [16] See Supplemental Material at <http://link.aps.org/supplemental/10.1103/PhysRevB.107.054106> for full details of structural measurements and data treatment, as well as a detailed comparison of models used in previous literature.
- [17] C. Murayama, M. Okabe, D. Urushihara, T. Asaka, K. Fukuda, M. Isobe, K. Yamamoto, and Y. Matsushita, Crystallographic features related to a van der Waals coupling in the layered chalcogenide $FePS_3$, *J. Appl. Phys.* **120**, 142114 (2016).
- [18] N. V. Y. Madsen, I. C. and Scarlett, Quantitative phase analysis. in *Powder Diffraction - Theory and Practice*, edited by S. J. L. Dinnabier and R. E. Billinge (Royal Society of Chemistry, London, 2008).
- [19] A. Coelho, TOPAS-ACADEMIC version 6 technical reference (2016), <http://topas-academic.net>.

- [20] P. W. Stephens, Phenomenological model of anisotropic peak broadening in powder diffraction, *J. Appl. Crystallogr.* **32**, 281 (1999).
- [21] C. Buchsbaum and M. U. Schmidt, Rietveld refinement of a wrong crystal structure, *Acta Crystallogr., Sect. B* **63**, 926 (2007).
- [22] G. W. Stinton and J. S. O. Evans, Parametric Rietveld refinement, *J. Appl. Crystallogr.* **40**, 87 (2007).
- [23] G. I. Lampronti, A. A. L. Michalchuk, P. P. Mazzeo, A. M. Belenguer, J. K. M. Sanders, A. Bacchi, and F. Emmerling, Changing the game of time resolved X-ray diffraction on the mechanochemistry playground by downsizing, *Nat. Commun.* **12**, 6134 (2021).
- [24] H. K. Mao, J. Xu, and P. M. Bell, Calibration of the ruby pressure gauge to 800 kbar under quasi-hydrostatic conditions, *J. Geophys. Res. Solid Earth* **91**, 4673 (1986).
- [25] D. J. Goossens, D. James, J. Dong, R. E. Whitfield, L. Norén, and R. L. Withers, Local order in layered NiPS₃ and Ni_{0.7}Mg_{0.3}PS₃, *J. Phys.: Condens. Matter* **23**, 065401 (2011).
- [26] A. R. Wildes, V. Simonet, E. Ressouche, G. J. McIntyre, M. Avdeev, E. Suard, S. A. J. Kimber, D. Lançon, G. Pepe, B. Moubaraki, and T. J. Hicks, Magnetic structure of the quasi-two-dimensional antiferromagnet NiPS₃, *Phys. Rev. B* **92**, 224408 (2015).
- [27] M. A. McGuire, Crystal and magnetic structures in layered, transition metal dihalides and trihalides, *Crystals* **7**, 121 (2017).
- [28] S. Son, M. J. Coak, N. Lee, J. Kim, T. Y. Kim, H. Hamidov, H. Cho, C. Liu, D. M. Jarvis, P. A. C. Brown, J. H. Kim, C.-H. Park, D. I. Khomskii, S. S. Saxena, and J.-G. Park, Bulk properties of the van der Waals hard ferromagnet VI₃, *Phys. Rev. B* **99**, 041402(R) (2019).
- [29] Y. Yin, X. Ma, D. Yan, C. Yi, B. Yue, J. Dai, L. Zhao, X. Yu, Y. Shi, J.-T. Wang, and F. Hong, Pressure-driven electronic and structural phase transition in intrinsic magnetic topological insulator MnSb₂Te₄, *Phys. Rev. B* **104**, 174114 (2021).
- [30] T. K. Chau, S. J. Hong, H. Kang, and D. Suh, Two-dimensional ferromagnetism detected by proximity-coupled quantum Hall effect of graphene, *npj Quantum Mater.* **7**, 27 (2022).
- [31] S. Calder, A. V. Haglund, Y. Liu, D. M. Pajerowski, H. B. Cao, T. J. Williams, V. O. Garlea, and D. Mandrus, Magnetic structure and exchange interactions in the layered semiconductor CrPS₄, *Phys. Rev. B* **102**, 024408 (2020).
- [32] V. Grasso and L. Silipigni, Low-Dimensional Materials: The MPX₃ Family Physical Features and Potential Future Applications, *Rivista Del Nuovo Cimento* **25**, 1 (2002).
- [33] Y. Guo, R. B. Smith, Z. Yu, D. K. Efetov, J. Wang, P. Kim, M. Z. Bazant, and L. E. Brus, Li intercalation into graphite: Direct optical imaging and Cahn–Hilliard reaction dynamics, *J. Phys. Chem. Lett.* **7**, 2151 (2016).
- [34] T. E. Weller, M. Ellerby, S. S. Saxena, R. P. Smith, and N. T. Skipper, Superconductivity in the intercalated graphite compounds C₆Yb and C₆Ca, *Nat. Phys.* **1**, 39 (2005).
- [35] H. K. Mao, R. J. Hemley, Y. Wu, A. P. Jephcoat, L. W. Finger, C. S. Zha, and W. A. Bassett, High-Pressure Phase Diagram and Equation of State of Solid Helium from Single-Crystal X-Ray Diffraction to 23.3 GPa, *Phys. Rev. Lett.* **60**, 2649 (1988).
- [36] M. J. Coak, S. Son, D. Daisenberger, H. Hamidov, C. R. S. Haines, P. L. Alireza, A. R. Wildes, C. Liu, S. S. Saxena, and J.-G. Park, Isostructural Mott transition in 2D honeycomb antiferromagnet V_{0.9}PS₃, *npj Quantum Mater.* **4**, 38 (2019).